The precursory phase of large earthquakes

Quentin Bletery, Jean-Mathieu Nocquet

The precursory phase of large earthquakes

Quentin Bletery[1,*] and Jean-Mathieu Nocquet[1,2]

[1]Universite Côte d'Azur, IRD, CNRS, Observatoire de la Côte d'Azur, Géoazur, France
[2]Institut de Physique du Globe de Paris, Université de Paris, CNRS, France

*To whom correspondence should be addressed; e-mail: bletery@geoazur.unice.fr

The existence of an observable precursory phase of slip on the fault before large earthquakes has been debated for decades. Though observations preceding a handful of large earthquakes have been proposed as possible indicators of precursory slip, these observations do not directly precede earthquakes, are not seen before most events and are also commonly observed without being followed by earthquakes. We conducted a global search for short term precursory slip in GPS data. We sum the displacements measured by 3,026 high-rate GPS time series – projected onto the directions expected from precursory slip at the hypocenter – during 48 hours before 90 (Magnitude ≥ 7) earthquakes. Our approach reveals a ≈ 2 h-long exponential acceleration of slip before the ruptures, suggesting that large earthquakes start with a precursory phase of slip, which improvements in measurement precision and density could more effectively detect and possibly monitor.

Main text

Introduction

Detecting precursors to natural disaster is key for predicting those events and minimizing human and economic losses. The search for earthquake precursors has been a long-standing pursuit, with a lot of hope being placed in the concept of earthquake prediction in the early 1970s (1). The potential for earthquake prediction was later seriously reassessed as theoretical studies suggested that earthquakes are non-linear processes that are highly sensitive to the unmeasurably fine details of the physical conditions at depth (*2,3*). In the last decade, the idea has grown that large earthquakes initiate with a potentially observable slow aseismic phase of slip on the fault, associated with increased micro-seismicity (*4–18*). Based on either geodetic or seismic data, these studies suggest that earthquake precursors exist and that therefore earthquakes could be anticipated minutes (*4*), days (*5,7,15,18*), weeks (*6*), months (*7–12*) or even years (*13*) before they occur.

Nevertheless, all these analyses are based on records preceding only a handful of earthquakes, strongly limiting the generalization of the observation. Moreover, slow aseismic slip events associated with increased micro-seismicity are routinely observed and most of the time do not precede a large earthquake (*19–24*), further questioning the causal relationship between these proposed precursory signals and the earthquakes. Another critical point is that these observations on natural faults do not show a continuous process culminating in the earthquake. Indeed, whether the observations come from geodetic or seismic data, they show evidence of a slow slip or a micro-seismic crisis usually stopping days or weeks before the catastrophic event (*4–6,8–18*). None of these observations shows an exponential build-up of the aseismic slip leading to the rupture, which is expected from laboratory experiments (*25–28*) and numerical models (*29–31*). One exception is a global analysis of the seismicity

preceding large earthquakes, which does find an exponential increase in the number of earthquakes ranging from years up to hours preceding large events (*7*).

Global stack of high-rate GPS data preceding large earthquakes

We investigated the existence of precursory signals in high-rate (5-min) GPS data recorded in the 48 hours preceding Mw ≥7.0 earthquakes worldwide (Fig. 1). We quantitatively test the hypothesis that earthquakes start with a precursory phase of slow aseismic slip at the location of the hypocenter of the forthcoming event. We calculate the expected displacements measured by GPS stations induced by such precursory slip (32). For each earthquake i, for each station j, at each time step t, we then calculate the dot product of the observed horizontal displacement $\overrightarrow{u_{i,j}}(t)$ with the horizontal displacement $\overrightarrow{g_{i,j}}$ expected from a unit precursory slip in the direction of the impending earthquake. If the observation is consistent with precursory slip – i.e. if $\overrightarrow{u_{i,j}}(t)$ and $\overrightarrow{g_{i,j}}$ have similar orientations – then the dot product will be positive. If GPS data do not contain any signal related to precursory slip, the dot product $\overrightarrow{u_{i,j}}(t) \cdot \overrightarrow{g_{i,j}}$ is equally likely to be positive or negative.

Using the global catalog of GPS data processed by the Nevada Geodetic Laboratory (*33*), we calculate this dot product, for each earthquake, for each station and then sum their contributions, at each (5 min) time step (with respect to the earthquake origin times), to obtain the stack time series,

$$S(t) = \sum_{i=1}^{N_{eq}} \sum_{j=1}^{N_{st}(i)} \frac{\vec{u}_{i,j}(t) \cdot \vec{g}_{i,j}}{\sigma_{i,j}^2}, \quad (1)$$

in the two days preceding the earthquake origin times, where $\sigma_{i,j}$ is an estimate of the noise amplitude at each station (32). Division by the square of the noise amplitude provides a weighted stack (*34–36*). Note that the dot product with the expected displacement field $\overrightarrow{g_{i,j}}$ gives a greater weight to measurements at stations where larger displacement is expected from precursory slip, i.e. at stations located close to the hypocenter of the upcoming

earthquake. If GPS data do not contain any earthquake precursory signal, we expect S to exhibit no obvious trend. Coherent noise structures reminiscent of colored noise in GPS data are expected to be strongly attenuated by the stack on multiple earthquakes, which should not share coherent noise patterns. Consistently, the distribution of S as a function of time shows no obvious coherent pattern from 48 to 2 hours before the earthquakes (Fig. 2A). However, in the 2 hours preceding the events, the stack reveals a positive trend supporting the hypothesis of a growing slip in the hypocenter area (Fig. 2A).

Statistical analysis of potential precursory signals

In order to reduce the high-frequency noise level, we calculate a moving average using time windows of 1 hour and 50 min (Fig. 2B). We find that the maximum of the moving average is the last point (i.e. the average of the stack in the 1 hour and 50 min preceding the earthquakes). Its ratio to the maximum of the stack moving average in the last 2 days (excluding the latest 1 h 50 min) is 1.82 (a moving median gives a slightly larger ratio of 2.1). The likelihood that the last point of the moving average is the largest by chance is less than 0.2% (32). The likelihood that the last point of the moving average is twice larger than the maximum on the [-48, -2] h time period is even much smaller. The ratio between the last point of the moving average and the standard deviation of the stack moving average in the last 2 days (excluding the latest 1 h 50 min) provides an estimate of the signal-to-noise ratio and is equal to 3.85 (3.9 with a moving median). Moreover, we find that the last 23 points of the moving average monotonically increase and the last 7 points exceed the maximum in the [-48, -2] h period. This means that these last 7 points of the moving average are larger than all values in the 48 hours before them. We perform the analysis on 100,000 random time windows of GPS data not preceding earthquakes. The last point of the moving average exceeds 1.82 and the 23 last points monotonically increases (the value found before the earthquakes) for only 0.03% of the

drawn samples (32), providing a rough estimate of the likelihood that the signal we observe arises from noise.

S is well fitted by an exponential function of time constant τ = 1.3 h (Fig. 2C). The misfit reduction of the fitted exponential function in the last 1 h 50 min is 79% (32), meaning that 79% of the signal in the last 1 h 50 min of S is explained by an exponential function. To facilitate interpretation, S can be converted into cumulative moment of preslip through a simple coefficient of proportionality (32). The exponential fit in moment can then be seen as a template of precursory (cumulative) moment release on the fault, suggesting that on average earthquakes have an exponential-like precursory phase as predicted by laboratory experiments (*25–28*) and dynamic models (*29–31*). The average cumulative moment obtained before the rupture (i.e. the last point in Figure 2.c) is 3.9×10^{18} N.m, corresponding to a moment magnitude of 6.3. Interestingly, such a magnitude and duration locate precursory slip in the observation gap of fault slip phenomena between slow aseismic slip and earthquakes (*37*). A more subtle, but noticeable, feature in S is a long period oscillation. The best sinusoidal fit to S (Fig. 2D) gives a period of 12.9 h, close to the period of tides (12.4 h). The misfit reduction of the fitted sinusoidal function is however only 10%, making the sinusoidal signal in S much less obvious than the exponential one.

In order to test if the observed signals are related to fault slip in the area of the forthcoming earthquakes, we replace $\overrightarrow{g_{i,j}}$ by unit vectors pointing to arbitrary fixed directions; for simplicity the east and north directions (32). The stack we obtain shows no signal similar to what we observe in the last 2 h of S, nor long-period oscillation (Fig. S1). This rules out that the shape of S results from a spatially correlated common mode error in GPS data, and strongly supports that the source of the signals observed in S is related to processes taking place in the direct vicinity of the hypocenter of the impending earthquakes.

The case of the Tohoku-Oki earthquake

The Tohoku-Oki earthquake (2011, Mw 9.0) is the largest event in our dataset. The event was also recorded by the largest number of stations (355 full time series) and is one of the handful of events for which short-term precursory activity was suggested by micro-seismicity analyses (*5*). We show the dot product stack for the Tohoku-Oki earthquake alone S_{TO} in the 24 h preceding the event (Fig. 3). S_{TO} suggests precursory slip similar to S. It also reveals an unexpected but relatively clear sinusoidal shape. As for the global stack, we verify that when replacing $\overrightarrow{g_{i,j}}$ by unit vectors pointing in the east and north directions, the signal vanishes (Fig. S2), strongly suggesting that this sinusoidal behavior is not related to GPS noise but is rather caused by processes taking place in the direct vicinity of the hypocenter of the Tohoku-Oki earthquake.

We find that the best fit for S_{TO} is a sinusoidal function of period T = 3.6 h. The misfit reduction for the 24 h time series is 72%. We try to fit sinusoidal functions to dot product stacks calculated at 833 randomly selected 48h-long time windows and find 0 fit for which the misfit reduction is as high at periods below 12 h (32). We also try to fit sinusoidal functions to dot product stacks calculated changing the location of the synthetic source (32) and find 0 source location giving a misfit reduction as high as for the location of the Tohoku earthquake (Fig. S11A). This means that, exploring both time and space, the most periodic signal obtained in S_{TO} is found right before the event, considering a source located at the location of the hypocenter (32). We do not believe that sinusoidal slip has been observed on natural faults before, but similar phenomena have been observed before glacier break-off (*38,39*). More precisely glacier precursory signals are log-periodic, meaning that the oscillation period decreases when getting closer to the rupture and the amplitude increases (*38,39*). Log periodic precursory activity also arises from earthquake rupture models (*40, 41*). As for the global stack, we convert S_{TO} into moment which can be seen as an (integrated) precursory source time

function. The amplitude of the fitted sinusoid is 1.0×10^{19} N.m, corresponding to a moment magnitude of 6.6. This large hypothetical precursory oscillation resembles the resonance effect predicted by rate-and-state friction laws when the fault approaches its critical state (*42*). The residual of S_{TO} with the sinusoid can be fitted by an exponential of time constant T_{TO} = 1.5 h, similar to the global stack. The associated cumulative moment release is 2.9×10^{19} N.m, corresponding to a moment magnitude of 6.9.

Contributions of individual earthquakes

Because the signal is large in S_{TO} and has a potentially large weight in S, we verify that when removing S_{TO} from the stack, the signal is still present (Fig. S3). We generalize the process and evaluate the relative contribution of each earthquake in the signal observed in the last 2 h and in the overall stack (32). We find that the signal is not overly dominated by one or a few earthquakes even though we see larger contributions from earthquakes recorded by many stations and by stations located close to the source of the impending earthquakes (Fig. S4). In details, 52 earthquakes (58% of the total) contribute positively to the global stack during the last 2 hours, but these 52 earthquakes represent 2,235 time series (74% of the time series) (32). Additionally, we calculated the average of the last 2h for the stacks on all earthquakes and found very similar figures: 54 earthquakes (60%) have a positive mean in the last 2 h of the stack, but these 54 earthquakes represent 2,251 time series (74% of the total).

Discussion

As the exponential function is always positive and monotonically increasing, a potential exponential acceleration of slip in the direction of the upcoming coseismic slip would sum constructively, making it likely to appear in the global stack. To the contrary, the oscillation properties of the sinusoidal function make a potential sinusoidal pre-slip unlikely to appear in

a multi-earthquake stack. Nonetheless, the global stack exhibits a weak sinusoidal signal. Even though the misfit reduction provided by the sinusoidal fit is only 10%, the best-fitting function has 2 interesting properties: (i) its period (12.9 h) is very close to the period of tides (12.4 h) and (ii) its value at the earthquake origin time is close to its maximum (Fig. 2D). These two properties can potentially explain how stacked oscillations could interfere positively: a common excitation source could result in a common excited period and an earthquake triggering at the most favorable time could explain the absence of phase lag. Correlations have been observed between tides and micro-seismicity (*43,44*), suggesting tidal modulation of slow aseismic slip (*45,46*). Correlations between tides and earthquakes have also been observed in time periods preceding large earthquakes, suggesting that when the faults are approaching the critical stage of failure, tidal loading may initiate a rupture (*47,48*). A 12 h oscillation on the faults in the days preceding the events is therefore physically consistent with a tidal excitation of the system, possibly enhanced by a resonance effect (*42*), as the faults reach their critical state.

Conclusion

Our analysis indicates that, on average, earthquakes start with a ≈ 2h-long exponential-like acceleration of slow slip. Analysis of foreshock activity also suggests exponential acceleration of fault slip but over a much wider range of time scales (*7*). The observation we make on GPS time series might be the very end of much a longer process of precursory slip. Though present instrumental capacities do not allow to identify precursory slip at the scale of individual earthquakes, our observation suggests that precursory signals exist and that the precision required to monitor them is not orders of magnitudes away from our current capabilities.

References

1. C. H. Scholz, L. R. Sykes, Y. P. Aggarwal, *Science* 181, 803 (1973).
2. Y. Y. Kagan, *Geophysical Journal International* 131, 505 (1997).
3. R. J. Geller, *Geophysical Journal International* 131, 425 (1997).
4. M. Bouchon, *et al.*, *science* 331, 877 (2011).
5. A. Kato, *et al.*, *Science* 335, 705 (2012).
6. S. Ruiz, *et al.*, *Science* 345, 1165 (2014).
7. M. Bouchon, V. Durand, D. Marsan, H. Karabulut, J. Schmittbuhl, *Nature geoscience* 6, 299 (2013).
8. B. Schurr, *et al.*, *Nature* 512, 299 (2014).
9. M. Bouchon, *et al.*, *Nature Geoscience* 9, 380 (2016). 10. M. Radiguet, *et al.*, *Nature Geoscience* 9, 829 (2016).
11. J. R. Bedford, *et al.*, *Nature* 580, 628 (2020).
12. A. Socquet, *et al.*, *Geophysical Research Letters* 44, 4046 (2017).
13. A. P. Mavrommatis, P. Segall, K. M. Johnson, *Geophysical Research Letters* 41, 4486 (2014).
14. E. E. Brodsky, T. Lay, *Science* 344, 700 (2014).
15. S. Ruiz, *et al.*, *Geophysical Research Letters* 44, 10 (2017).
16. W. L. Ellsworth, F. Bulut, *Nature Geoscience* 11, 531 (2018).

17. C. Tape, *et al.*, *Nature Geoscience* 11, 536 (2018).

18. E. Caballero, *et al.*, *Geophysical research letters* 48, e2020GL091916 (2021).

19. S. Y. Schwartz, J. M. Rokosky, *Reviews of Geophysics* 45 (2007).

20. J. Gomberg, C. 2007, B. W. Group, *Bulletin* 122, 963 (2010).

21. K. Obara, A. Kato, *Science* 353, 253 (2016).

22. Q. Bletery, J.-M. Nocquet, *Nature communications* 11, 1 (2020).

23. L. M. Wallace, *Annual Review of Earth and Planetary Sciences* 48, 175 (2020).

24. W. M. Behr, R. Bürgmann, *Philosophical Transactions of the Royal Society A* 379, 20200218 (2021).

25. M. Ohnaka, L.-f. Shen, *Journal of Geophysical Research: Solid Earth* 104, 817 (1999).

26. S. Latour, A. Schubnel, S. Nielsen, R. Madariaga, S. Vinciguerra, *Geophysical Research Letters* 40, 5064 (2013).

27. F. X. Passelègue, *et al.*, *Fault zone dynamic processes: Evolution of fault properties during seismic rupture* pp. 229–242 (2017).

28. C. Hulbert, *et al.*, *Nature Geoscience* 12, 69 (2019).

29. J. H. Dieterich, B. Kilgore, *Proceedings of the National Academy of Sciences* 93, 3787 (1996).

30. A. M. Rubin, J.-P. Ampuero, *Journal of Geophysical Research: Solid Earth* 110 (2005).

31. Y. Kaneko, S. B. Nielsen, B. M. Carpenter, *Journal of Geophysical Research: Solid Earth* 121, 6071 (2016).

32. Materials and Methods are available as Supplementary Materials on Science Online.

33. G. Blewitt, W. C. Hammond, C. Kreemer, *Eos* 99, 485 (2018).

34. T. R. Stevenson, *Physical Review D* 56, 564 (1997).

35. Y. Tyapkin, B. Ursin, *Journal of Geophysics and Engineering* 2, 177 (2005).

36. J.-P. Montagner, *et al.*, *Nature communications* 7, 1 (2016).

37. S. Ide, G. C. Beroza, D. R. Shelly, T. Uchide, *Nature* 447, 76 (2007).

38. J. Faillettaz, A. Pralong, M. Funk, N. Deichmann, *Journal of Glaciology* 54, 725 (2008).

39. J. Faillettaz, M. Funk, C. Vincent, *Reviews of Geophysics* 53, 203 (2015).

40. D. Sornette, C. G. Sammis, *Journal de Physique I* 5, 607 (1995).

41. R. C. Viesca, *Physical Review E* 93, 060202 (2016).

42. H. Perfettini, J. Schmittbuhl, J. R. Rice, M. Cocco, *Journal of Geophysical Research: Solid Earth* 106, 13455 (2001).

43. J. L. Rubinstein, M. La Rocca, J. E. Vidale, K. C. Creager, A. G. Wech, *Science* 319, 186 (2008).

44. A. M. Thomas, R. M. Nadeau, R. Bürgmann, *Nature* 462, 1048 (2009).

45. J. C. Hawthorne, A. M. Rubin, *Journal of Geophysical Research: Solid Earth* 115 (2010).

46. H. Houston, *Nature Geoscience* 8, 409 (2015).

47. S. Tanaka, *Geophysical Research Letters* 37 (2010).

48. S. Tanaka, *Geophysical research letters* 39 (2012).

49. github.com/QuentinBletery/Bletery_and_Nocquet_Science_2023, doi:

50. geodesy.unr.edu

Acknowledgments

We are grateful to Jean-Paul Ampuero, Guust Nolet, Geoffrey Blewitt, Jean-Philippe Avouac, Diane Rivet, Cédric Twardzik and François Passelègue for helpful discussion.

Funding: This project has received funding from the European Research Council (ERC) under the European Union's Horizon 2020 research and innovation programme (grant agreement 949221) and from the French National Research Agency (grant agreement ANR-19-CE310003).

Author Contributions: Q.B. had the original idea. J.M.N. provided numerical tools (PYACS python library) and expertise on GNSS data. Both authors contributed to the analysis, interpretation and to the preparation of the manuscript.

Competing Interests: The authors declare that they have no competing interests.

Data and Material availability: All the scripts and data used to perform this study are available online (49). The pyacs library we used for data processing and Green's functions calculation is available in the following webpage: github.com/JMNocquet/pyacs36. The GPS time series we used are available on the website of the Nevada Geodetic Laboratory of the University of Nevada Reno (50).

Supplementary materials

Materials and Methods

Figs. S1 to S11

References *(51-53)*

Figure 1: Earthquakes and GPS stations used in the study. Upper panel: Distribution and focal mechanisms of the 90 Mw ≥ 7 earthquakes with 2 days of 5-min GPS records (with no gap and no noticeable foreshock) available within a 500 km radius of the epicenters. Mechanism sizes are indicative of event magnitudes. Colors indicate the number of time series available for each event. Lower panel: Distribution of the 3,026 GPS stations with complete records in the 2 days preceding the 90 earthquakes shown above. Sub-panels are zooms on areas of high station concentration.

Figure 2: Global stack in the direction of expected slip. (A) Global stack S of 3,026 time series recorded before 90 earthquakes as a function of time relative to each earthquake origin time. (B) 1h50min-moving average of S normalized by its standard deviation on the [-48h, -1h50] time period, superimposed on S. The upper horizontal dashed line indicates the maximum of the moving average (excluding the last 1h50min). The lower horizontal dashed line indicates the 0 base line (above which observations are consistent with precursory slip). The vertical dashed line indicates the time after which the stack gives only positive values (1 h and 55 min). The last point of the moving average is 1.82 times larger than the maximum on the [-48h, -1h50] time period and 3.85 times larger than the standard deviation, providing a rough estimate of the signal-to-noise ratio. (C) Stack converted into moment (see Supplementary materials) with best exponential fit superimposed (time constant τ = 1.3 h). (D) Stack in moment with best sinusoidal fit superimposed (period T = 1.9 h).

Figure 3: Stack in the direction of expected slip for Tohoku. (A) Stack of 355 time series recorded before the Tohoku-Oki earthquake. (B) Same as (A) converted in moment release with best sinusoidal fit superimposed (period T_{TO} = 3.6 h). (C) Residual of the moment release stack with the sinusoidal fit (blue dots) and best exponential fit (red curve, time constant τ_{TO} = 1.5 h).

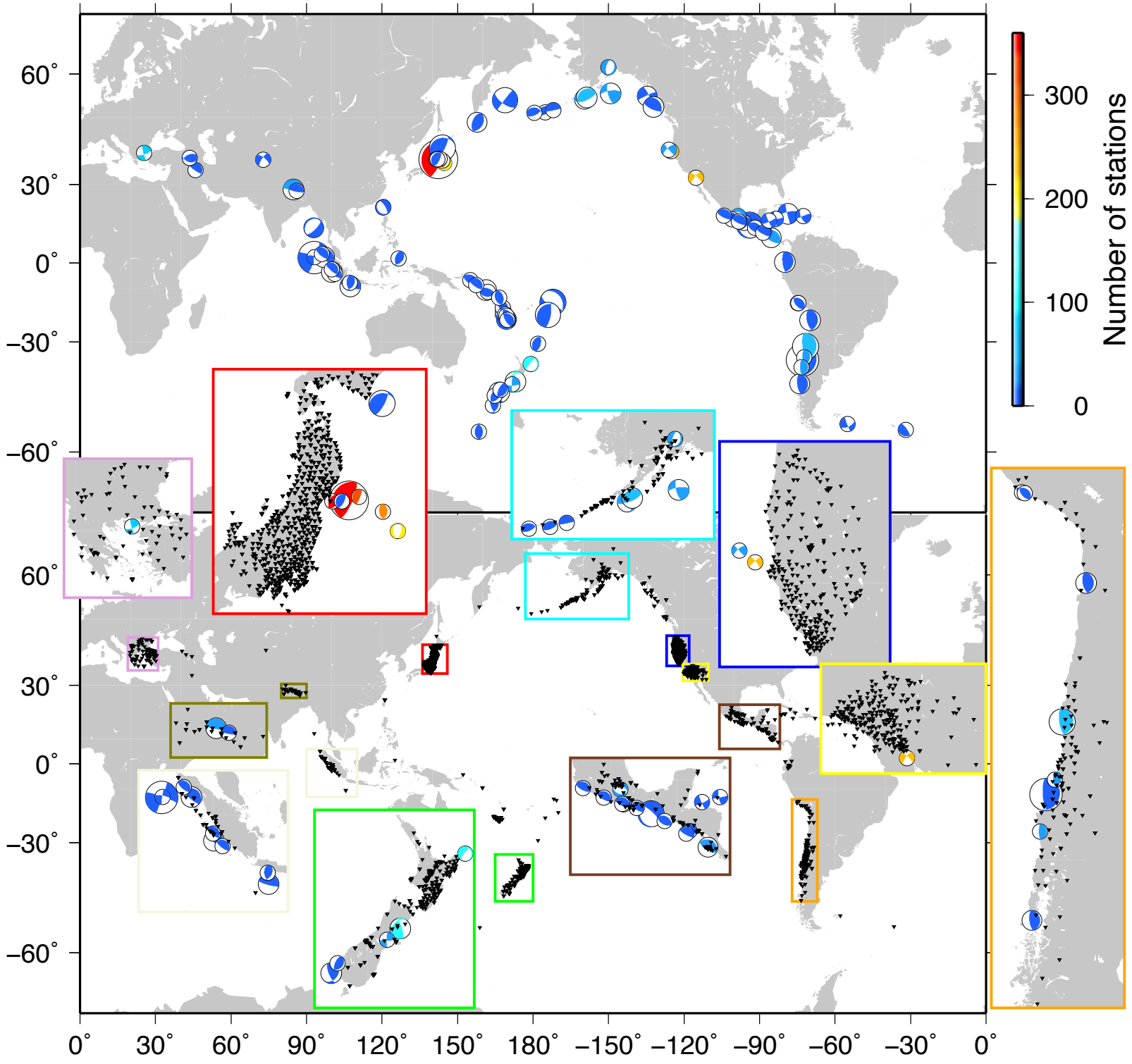
60°
30°
0°
−30°
−60°
0°
30°
60°
90°
120°
150°
180°
−150°
−120°
−90°
−60°
−30°
0°
300
200
100
0
Number of stations

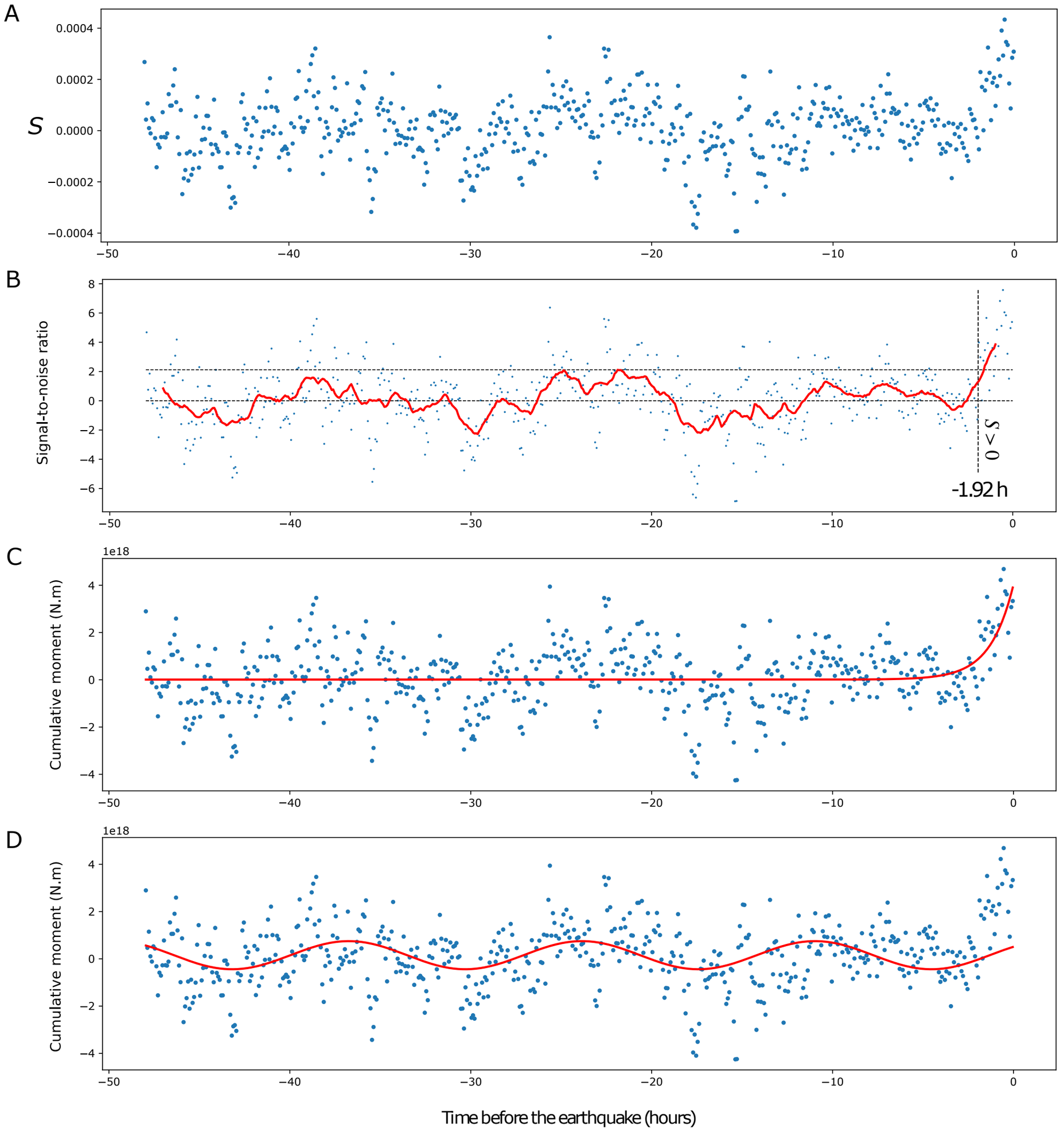
A
S
0.0004
0.0002
0.0000
−0.0002
−0.0004
−50
−40
−30
−20
−10
0
B
Signal-to-noise ratio
8
6
4
2
0
−2
−4
−6
S/N
-1.92 h
C
1e18
Cumulative moment (N.m)
D
1e18
Cumulative moment (N.m)
Time before the earthquake (hours)

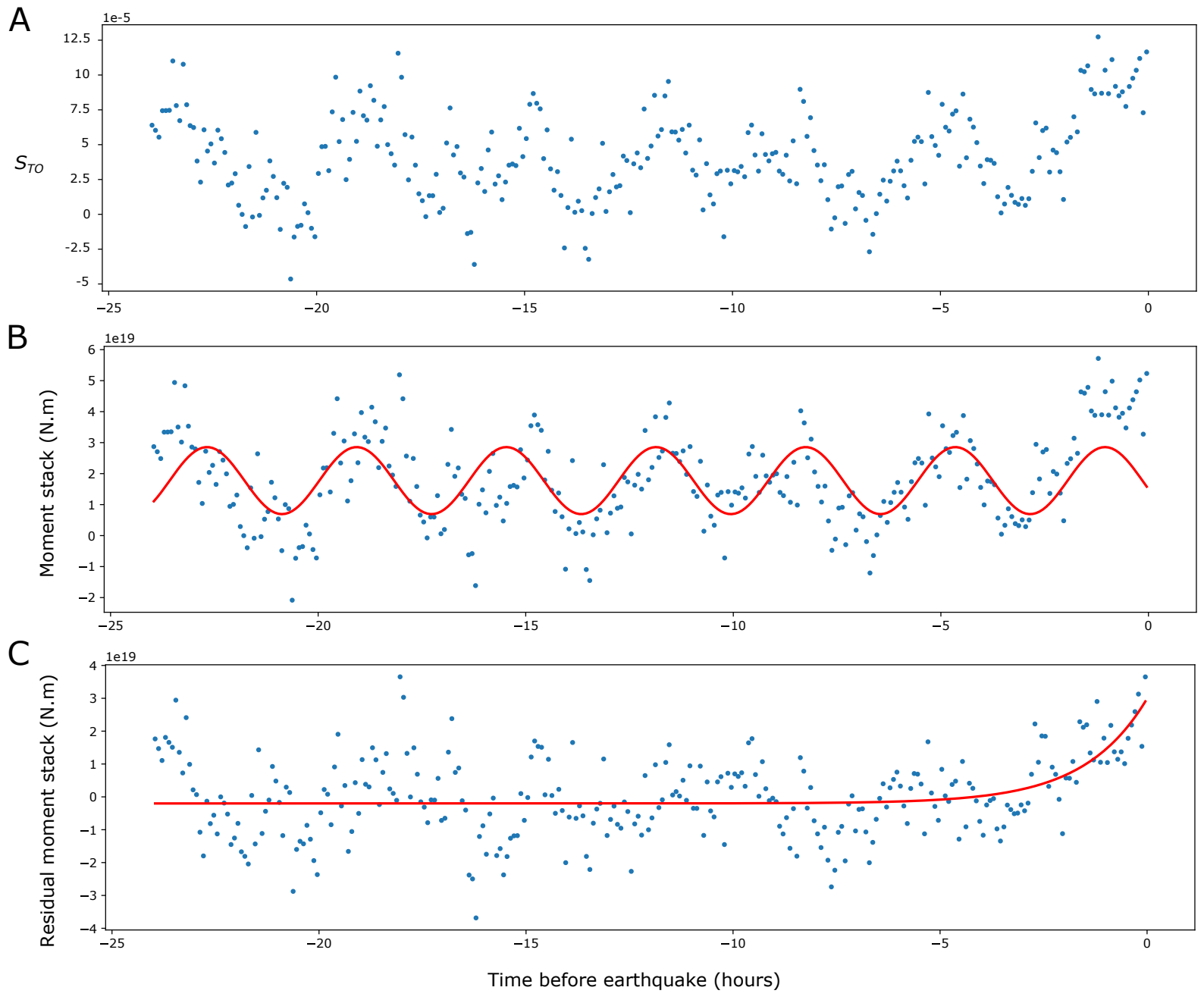
A
1e-5
12.5
10
7.5
5
2.5
0
-2.5
-5
S_{TO}
−25
−20
−15
−10
−5
0
B
1e19
6
5
4
3
2
1
0
−1
−2
Moment stack (N.m)
−25
−20
−15
−10
−5
0
C
1e19
4
3
2
1
0
−1
−2
−3
−4
Residual moment stack (N.m)
−25
−20
−15
−10
−5
0
Time before earthquake (hours)

Supplementary Materials for:

The precursory phase of large earthquakes

Quentin Bletery* and Jean-Mathieu Nocquet

*To whom correspondence should be addressed; E-mail: bletery@geoazur.unice.fr.

This PDF file includes:

Materials and methods

Data

We download the global dataset of 5-min GPS time series processed by the Nevada Geodetic Laboratory of the University of Nevada Reno *(33,50)*. Positions are estimated using kinematic Precise Point Positioning using carrier phase measurements decimated every 5 minutes. Very large process noise allowed in the kinematic processing ensures that coordinate estimates at successive 5-min epochs are independent, and that pre-earthquake positions are not influenced by the subsequent co-seismic motion (G. Blewitt, personal communication). We use the magnitudes, hypocenter locations, times and focal mechanisms given by the SCARDEC earthquake database (*51*) to select GPS time series preceding $M_w \geq 7$ earthquakes within a radius of 500 km from the hypocenters. To minimize potential biases, we only keep time series with no gap – i.e. containing full 576-sample time series in the 2 days preceding the events – and containing no noticeable foreshock in that time period (2 days before the events). We implement an automatic offset detector, which excludes 4 events preceded by significant foreshocks in the 2 days before the events : the 2019 Ridgecrest earthquake (M_w 7), the largest aftershock (M_w 7.7) of the 2014 Iquique earthquake and 2 earthquakes that happened on September 5 2004 in Japan. In total, our dataset is composed of 3,026 time series of 576 samples (2 days sampled at 5 min) recorded before 90 individual earthquakes (Table S1).

We define the 0 of the time series as the median of the positions between 48 and 24 hours before the earthquake. We therefore substract the median position in this time period from the 2-day time series to obtain $\vec{u}_{i,j}(t)$. We only use the horizontal component, therefore $\vec{u}_{i,j}(t)$ is a 2-component vector giving the east and north positions at time t relative to the median position on the previous day. We also estimate the noise amplitude on each station as the L2 norm of $\vec{u}_{i,j}(t)$ between 48 and 24 hours before the earthquake $\sigma_{i,j} = ||\vec{u}_{i,j}(t_{[-48,-24]})||$.

Weighted stack

We calculate the expected horizontal displacements at the station locations due to a unit of slip on a 1 km by 1 km fault defined by the hypocenter locations and focal mechanisms of the 90 earthquakes. To compute these "static Green's functions" $\vec{g}_{i,j}$, we consider a simple fault dislocation embedded in a homogeneous semi-infinite elastic half space (*52, 53*), with Lamé parameters $\lambda = 28.758$ GPa and $\mu = 29.353$ GPa, the fault geometry and slip direction being defined by the focal mechanism of the impending earthquake. We deliberately choose unrealistically small fault surfaces (1 km by 1 km), effectively equivalent to point sources, in order to limit modeling errors due to the nodal plane ambiguity. $\vec{g}_{i,j}$ is a 2-component vector giving the expected displacement recorded at station j for an earthquake i if the fault started slipping (of a unit of slip) at the location of the hypocenter of the upcoming earthquake, in the direction of upcoming slip.

For each earthquake i, for each station j, at each time step t, we calculate the dot product of $\vec{u}_{i,j}(t)$ with $\vec{g}_{i,j}$. If the measured position $\vec{u}_{i,j}(t)$ is consistent with slip expected from precursory slip at the earthquake location, i.e. if $\vec{u}_{i,j}(t)$ and $\vec{g}_{i,j}$ have similar orientations, then the dot product is going to be positive. If the measured position $\vec{u}_{i,j}(t)$ is inconsistent with slip expected from precursory slip at the earthquake location, i.e. if $\vec{u}_{i,j}(t)$ and $\vec{g}_{i,j}$ have opposite orientations, then the dot product is going to be negative. If $\vec{u}_{i,j}(t)$ and $\vec{g}_{i,j}$ are perpendicular, the dot product is going to be null. On average, if no precursory slip exists, we expect the dot product to be randomly distributed around zero. A natural weight arises from taking the dot product with $\vec{g}_{i,j}$. If station j is close to the source of earthquake i, then the norm of $\vec{g}_{i,j}$ is going to be large compared to more distant stations, and the amplitude of the dot product will naturally be larger.

At each time step t, we then calculate the stack $S(t)$ of the dot products obtained for each

station, for each earthquake :

$$S(t) = \sum_{i=1}^{N_{eq}} \sum_{j=1}^{N_{st}(i)} \frac{\vec{u}_{i,j}(t) \cdot \vec{g}_{i,j}}{\sigma_{i,j}^2}. \quad (1)$$

We divide each dot product by the square of our estimate of the noise amplitude on each station $\sigma_{i,j}^2 = ||\vec{u}_{i,j}(t_{[-48,-24]})||^2$ (*33-35*). We obtain the stack time series S shown in Fig. 2A.

Relation to fault slip and moment rate

Let s_i be the hypothetical precursory slip on the fault in the direction of the forthcoming co-seismic slip of a forthcoming earthquake i. By definition of $\vec{g}_{i,j}$,

$$\vec{g}_{i,j} s_i(t) = \vec{u}_{i,j}(t) \quad (S1)$$

Taking the dot product with $\vec{g}_{i,j}$ and dividing by $\sigma_{i,j}^2$, we have

$$\frac{\vec{g}_{i,j} \cdot \vec{g}_{i,j}}{\sigma_{i,j}^2} s_i(t) = \frac{\vec{g}_{i,j} \cdot \vec{u}_{i,j}(t)}{\sigma_{i,j}^2} \quad (S2)$$

Stacking on all stations and all earthquakes, we can write

$$\sum_{i=1}^{N_{eq}} \sum_{j=1}^{N_{st}(i)} \frac{\vec{g}_{i,j} \cdot \vec{g}_{i,j}}{\sigma_{i,j}^2} s_i(t) = S(t) \quad (S3)$$

Assuming the hypothetical pre-slip s_i is the same for every earthquake ($s_i = s$),

$$s(t) \sum_{i=1}^{N_{eq}} \sum_{j=1}^{N_{st}(i)} \frac{\vec{g}_{i,j} \cdot \vec{g}_{i,j}}{\sigma_{i,j}^2} = S(t). \quad (S4)$$

Writing $\sigma_g = \sum_{i=1}^{N_{eq}} \sum_{j=1}^{N_{st}(i)} \frac{\vec{g}_{i,j} \cdot \vec{g}_{i,j}}{\sigma_{i,j}^2}$, we obtain

$$s(t) = \frac{S(t)}{\sigma_g}. \quad (S5)$$

Since we arbitrarily impose the fault length (L) and width (W) in the calculation of $\vec{g}_{i,j}$ to 1 km, the obtained value of $s(t)$ is not relevant. A more relevant quantity is the corresponding cumulative moment,

$$M_0(t) = \mu L W s(t) = \frac{\mu L W}{\sigma_g} S(t), \quad (S6)$$

where $\mu = 29.353 \times 10^9$ Pa is the shear modulus and L = W = 10^3 m.

Stack time series analysis

We calculate a moving average of S using time windows of 1 hour and 50 min. Each point in Fig. 2B is the average of 22 points of S (11 before and 11 after), normalized by the standard deviation of the moving average in the time period unaffected by the 22 last points. We find that the last point of the moving average (corresponding to the average of S in the last 1 hour and 50 min before the earthquakes) is 1.82 times larger than the maximum of the moving average in the [-48, -2] h time period, and 3.85 times larger than its standard deviation. The likelihood that the last point of the moving average is the maximum by chance is one over the number of point in the time series, i.e. $1/553 = 0.18\%$. This statement can be made for the 7 last points of the moving average which are all larger than all the values before them. Replacing the moving average by a moving median gives the same shape with the last value 2.1 times larger than the maximum on the [-48, -2] h time period and 3.9 times larger than the standard deviation.

We search for the exponential function $y^e = a\exp(t/\tau) + b$ best fitting S (Fig. 2C) and obtain a time constant $\tau = 1.3$ h. The last point of the exponential fit exhibits a seismic moment of 3.9×10^{18} N.m, corresponding to a moment magnitude of 6.3. The misfit reduction associated with y^e, defined as $\frac{||S||^2 - ||S-y^e||^2}{||S||^2}$, is equal to 79% in the last 1 h 50 min.

We also search for the sinusoidal function $y^s = A\sin(\omega t + \phi) + B$ best fitting S and find a period $T = 2\pi/\omega = 12.9$ h and an amplitude $A = 5.9 \times 10^{17}$ N.m, corresponding to a moment magnitude of 5.8. The misfit reduction over the full 48 h time series is 10%.

We show in Fig. 3A the stack time series for the Tohoku-Oki earthquake alone :

$$S_{\text{TO}}(t) = \sum_{j=1}^{N_{st}(\text{TO})} \frac{\vec{u}_j(t) \cdot \vec{g}_j}{\sigma_j^2}. \tag{S7}$$

S_{TO} presents an obvious sinusoidal shape (Fig. 3A). We therefore search for the best-fitting sinusoidal function $y^s_{\text{TO}} = A_{\text{TO}}\sin(\omega_{\text{TO}} t + \phi_{\text{TO}}) + B_{\text{TO}}$ (Fig. 3B) after converting S_{TO} in moment (by dividing by $\sum_{j=1}^{N_{st}(\text{TO})} \frac{\vec{g}_j \cdot \vec{g}_j}{\sigma_j^2}$, see previous section). We obtain a period $T_{\text{TO}} = 2\pi/\omega_{\text{TO}} = 3.6$

h and an amplitude $A_{\text{TO}} = 1.0 \times 10^{19}$ N.m, corresponding to a moment magnitude of 6.6. The misfit reduction of y^s_{TO} is 72% in the [-24, 0] h time period. We then calculate the residual $S_{\text{TO}} - y^s_{\text{TO}}$ and fit an exponential function to it (Fig. 3C). We obtain a time constant $\tau_{\text{TO}} = 1.5$ h. The last point of the exponential fit exhibits a seismic moment of 2.9×10^{19} N.m, corresponding to a moment magnitude of 6.9.

Stack on fixed directions

To assess whether or not the obtained signal is associated to precursory slip in the hypocenter location of the upcoming earthquake, we perform the same stack but replacing $\vec{g}_{i,j}$ by unit vectors $\vec{e}$ and $\vec{n}$ pointing in the east and north directions respectively. For consistency with Fig. 2A, we set the amplitudes of $\vec{e}$ and $\vec{n}$ to the sum of the the amplitudes of the Green's functions. We obtain the east stack S^E and north stack S^N :

$$S^E(t) = \sum_{i=1}^{N_{eq}} \sum_{j=1}^{N_{st}(i)} \frac{\vec{u}_{i,j}(t) \cdot \vec{e}}{\sigma^2_{i,j}}, \tag{S8}$$

$$S^N(t) = \sum_{i=1}^{N_{eq}} \sum_{j=1}^{N_{st}(i)} \frac{\vec{u}_{i,j}(t) \cdot \vec{n}}{\sigma^2_{i,j}}. \tag{S9}$$

S^E and S^N show no obvious signal in the hours preceding the earthquakes (Fig. S1), strongly suggesting that the source of the signal observed in S is related to processes taking place in the direct vicinity of the hypocenter of the impending earthquakes.

We calculate the same way S^E_{TO} and S^N_{TO} for the specific case of the Tohoku-Oki earthquake,

$$S^E_{\text{TO}}(t) = \sum_{j=1}^{N_{st}(\text{TO})} \frac{\vec{u}_j(t) \cdot \vec{e}}{\sigma^2_j}, \tag{S10}$$

$$S^N_{\text{TO}}(t) = \sum_{j=1}^{N_{st}(\text{TO})} \frac{\vec{u}_j(t) \cdot \vec{n}}{\sigma^2_j}. \tag{S11}$$

S^E_{TO} and S^N_{TO} show some trends (Fig. S2). In particular S^E_{TO} shows a 3-h positive slope before origin time but similar slopes can be seen at other times in the time series (e.g. from -21 to -18

h). More importantly, no periodic signal similar to S_{TO} can be seen in either S_{TO}^E or S_{TO}^N (Fig. S2), suggesting that the source of the sinusoidal signal observed in S_{TO} is related to processes taking place in the direct vicinity of the hypocenter of the forthcoming earthquakes.

Contributions of individual earthquakes to the stack

We investigate the relative contribution of each earthquake to the stack. One way to evaluate the contribution of an event in S is to remove it from the stack. Doing this for the presumably most prominent earthquake in S, the Tohoku-Oki earthquake, we see that the acceleration of slip in the last 2 h is still present (Fig. S3). We generalize this approach by calculating the "contribution" $C_i^{\Delta T}$ of each earthquake i to the stack,

$$C_i^{\Delta T} = \frac{1}{a^{\Delta T}} \left(\sum_{t=-\Delta T}^{0} S(t)^2 - \sum_{t=-\Delta T}^{0} \left(S(t) - S_i(t)\right)^2 \right), \tag{S12}$$

where S_i is the stack of an individual earthquake i and $a^{\Delta T} = \sum_i C_i^{\Delta T}$ is a normalisation factor. Note that $C_i^{\Delta T}$ is negative when the contribution S_i of an earthquake i has an opposite trend to S. We calculate $C_i^{\Delta T}$ for the last 2 h (C_i^{2h}) and for the full 48 h (C_i^{48h}). C_i^{2h} is a measure of the relative contribution of each earthquake in the exponential-like signal observed in S before origin time. C_i^{48h} is a measure of the relative contribution of each earthquake in the entire stack. We also calculate $\sigma_i = \sum_{j=1}^{N_{st}(i)} \frac{\sqrt{\vec{g}_j \cdot \vec{g}_j}}{\sigma_{i,j}^2}$, which corresponds to the natural weights in the stack given by the dot product with $\vec{g}_j$.

We plot C_i^{2h} as a function of C_i^{48h}, with the dot sizes indicating σ_i (Fig. S4). We observe that C_i^{2h} correlates well with C_i^{48h} (correlation coefficient : 0.77) and with σ_i (correlation coefficient : 0.64), meaning that the exponential build-up we observe in the last 2 h mainly arises from contributions of earthquakes that have a large weight in the overall stack and large natural weights. We find that 3 earthquakes have a contribution above 10% in the last 2 h : the Tohoku-Oki (2011, M_w 9.0, 355 stations, $C_i^{2h} = 23.9\%$), the Baja California (2010, M_w 7.1, 236

stations, $C_i^{2h} = 20.7\%$) and the North California (2014, M_w 7.0, 246 stations, $C_i^{2h} = 21.8\%$) earthquakes. Two other earthquakes have an overall weight above 10% : the Kaikoura (2016, M_w 7.9, 97 stations, $C_i^{48h} = 11.2\%$) and the Nicoya (2012, M_w 7.5, 22 stations, $C_i^{48h} = 10.8\%$) earthquakes. Therefore, even though the relative contribution of individual events is far from being homogeneous, the observed signals in the stack are not overly dominated by one or a few earthquakes. Moreover, the earthquakes with the largest weights are earthquakes recorded by many stations and earthquakes recorded by stations located particularly close to the source (such as the Nicoya earthquake) – i.e., earthquakes that have large σ_i – which are the ones we expect to extract the most information from.

At the scale of individual earthquakes, no signal appears as clearly as in the global stack, even for the events with large C_i^{2h} (Fig. S5), meaning that stacking numerous earthquakes is necessary to reach a signal-to-noise ratio sufficiently high to see a possible pre-slip signal (individual plots for the full 90 events can be found in the GitHub repository under the eq_stack_figures directory). In fact, even looking at favorable examples, in favorable conditions, it is difficult to observe any trend in individual events. For illustration purposes, we represent in map view (Fig. S6A) the median displacement in the 2 hours preceding Tohoku (blue arrows) with respect to the median position in the [-48, -24] h time period, together with the synthetics displacements expected from precursory slip (red arrows). Fig. S6B shows the dot product between the blue and red arrows as a function of distance to the epicenter of the Tohoku earthquake. The amplitude of the dot product is larger at smaller distances mainly because the synthetic displacements have larger amplitudes. However, the sign of the dot product (systematically positive at distances shorter than 150 km) indicates that the observations are more and more consistent with pre-slip with increasing proximity to the impending source, even when normalizing by the amplitude of the Green's functions (Fig. S6C). To eliminate the possibility that the signal arises from a common mode noise, we subtract the common mode (stack of the raw time series divided by

the number of stations) to the raw time series and reproduce Fig. S6 (Fig. S7).

Dependence on station radius selection

We assess the impact of changing the station-hypocenter distance criterion we used to select the GPS time series considered in our global stack. To do so, we re-calculate the global stack considering only stations within 400, 300, 200 and 100 km from the epicenters of the forthcoming earthquakes (Fig. S8). We find that changing the radius for station selection does not affect much the obtained global stack (Fig. S8), because the amplitude of the Green's functions progressively damps the weight of the stations with distance.

Uniqueness of the signals we observe

To estimate the likelihood that the potential precursory signal we observe arises from noise, we apply the analysis presented above to 100,000 random time windows. We first draw a random time within every 6 hour window of the year each earthquake occurred, excluding the 2 days before the event and the 90 days after to limit contamination by afterslip signal. We then treat the randomly drawn times as the origin time of "fake earthquakes" and compute the dot product stack in the 48 preceding hours the same way we did in our analysis, if at least 75% of the stations have complete records in this time period. We then draw 100,000 random combinations of the dot product stacks for different earthquakes and stack them. We obtain 100,000 random realisations of S at times not preceding earthquakes. For each realisation, we calculate the moving average (of time window : 1h50min) and take the ratio r of its last point to its maximum in the 2 previous days. We obtain the histogram shown in Fig. S9A. We also count the number n of monotonically increasing points at the end of the moving average (Fig. S9B).

Over the 100,000 random obtained stacks, we find $r > 1.82$ (the value found in our analysis) in 0.27% of the cases and $n \geq 23$ in 0.82% of the cases. Both conditions are met only

for 0.03% of the drawn samples. This number can be seen as the likelihood that the signal we observe arises from noise. Note that this likelihood is likely over-estimated because a significant portion of the stacks for which one or both conditions are met contain obvious offsets which bias the test (all test plots can be found in the GitHub repository under the test_figures directory). Additionally, we find that the median value of the distribution of r is not null but slightly positive, which is likely due to post-seismic contamination of the samples we used to perform the test, and likely artificially increases the number of realisations with $r > 1.82$. Also, the number of available stations is significantly smaller than the 3,026 used in our analysis in all the tests, which decreases the expected signal-to-noise ratio, and also likely artificially increases the number of realisations with $r > 1.82$.

We perform a similar test to estimate the likelihood that the signal we observe before the Tohoku earthquake is due to high-frequency noise. We try to fit sinusoidal functions to the 833 test stack time series calculated at random times for the previous test on the Tohoku stations. Over the 833 stacks, the misfit reduction exceeds 60% only 29 times (the plots of the 29 fits can be found in the GitHub repository, under the figures_tohoku_test folder). The period of these 29 fits is below 10 hours in only 5 cases (shown in Fig. S10). In none of these cases does the misfit reduction exceed the one we found before the Tohoku event (72%). Moreover, none of them gives the visual impression of sinusoidal signal we observe in Fig. 3 (Fig. S10).

Additionally, we investigate the sensitivity of both the periodic and exponential signals we observe before the Tohoku earthquake to the source location. We recalculate the dot product stack using Green's functions computed considering different source locations. We then search for the sinusoidal function best fitting the obtained stacks (without fixing the period) and calculate the misfit reduction provided by the sinusoidal fits. We obtain the largest value (72%) for the location of the Tohoku earthquake (Fig. S11A), indicating that the source of the periodic signal we observe before the event (Fig. 3B) is in the direct vicinity of the hypocenter of the im-

pending Tohoku earthquake. We also calculate the mean value in the last 2 hours for the stacks calculated considering different source locations and similarily observe that the largest values are obtained at the location of the Tohoku earthquake, or at locations close to it (Fig. S11B).

Supplementary references

51. M. Vallée, V. Douet, *Physics of the Earth and Planetary Interiors* **257**, 149 (2016).

52. L. Mansinha, D. Smylie, *Bulletin of the Seismological Society of America* **61**, 1433 (1971).

53. Y. Okada, *Bulletin of the seismological society of America* **75**, 1135 (1985).

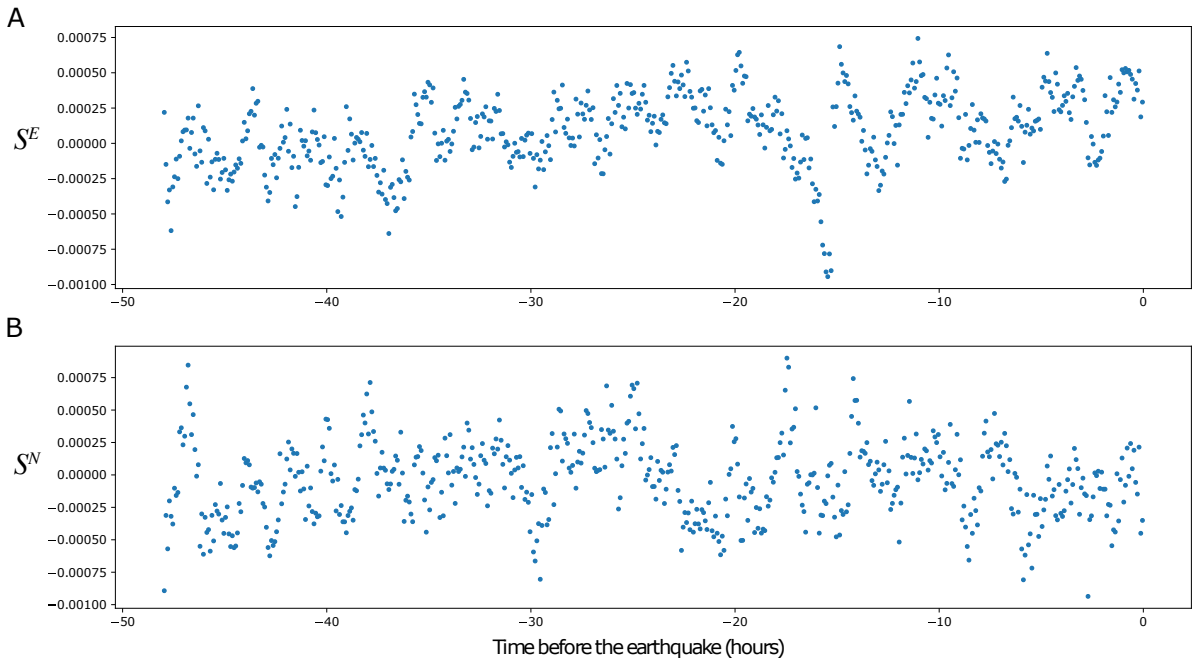

FIGURE S1 – **Global stack in the east and north directions.** (A) Global stack of the GPS time series preceding each earthquake projected in the east direction. (B) Same as (A) but projected in the north direction.

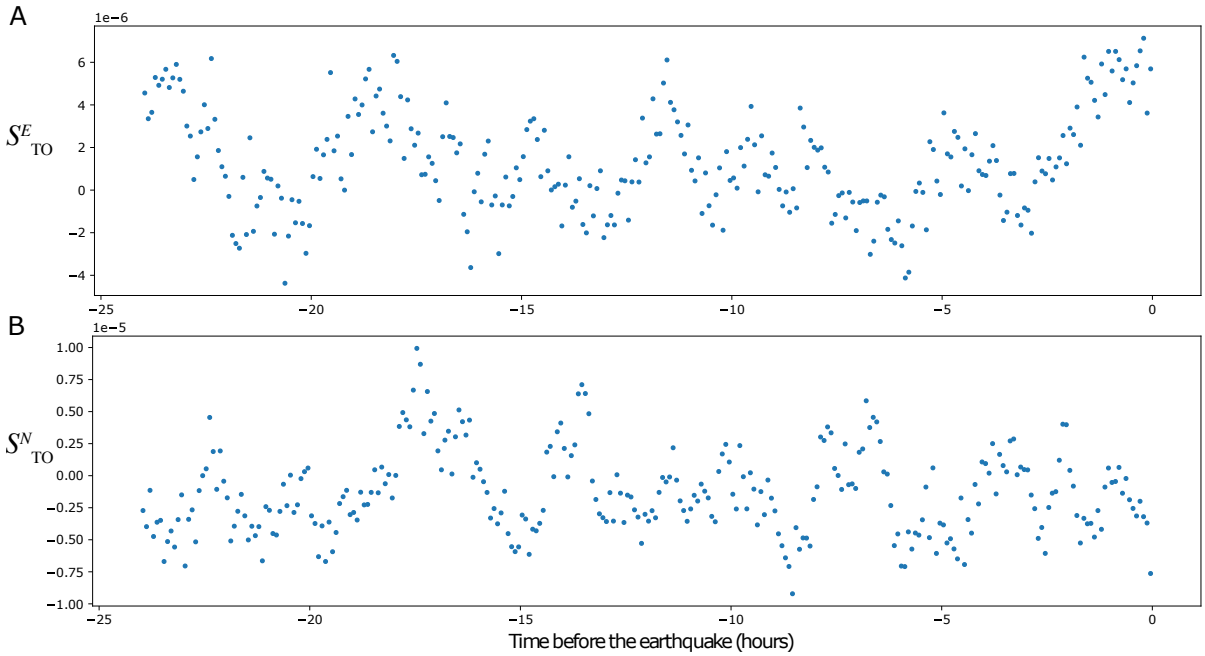

FIGURE S2 – **Stack in the east and north directions for Tohoku.** (A) Stack of the GPS time series preceding the Tohoku-Oki earthquake projected in the east direction. (B) Same as (A) but projected in the north direction.

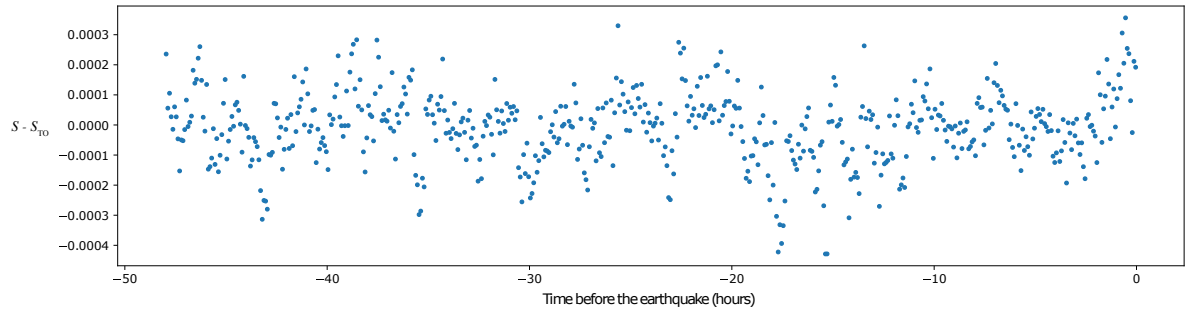

FIGURE S3 – **Global stack without Tohoku.** Same as Fig. 2A removing the Tohoku-Oki earthquake from the stack.

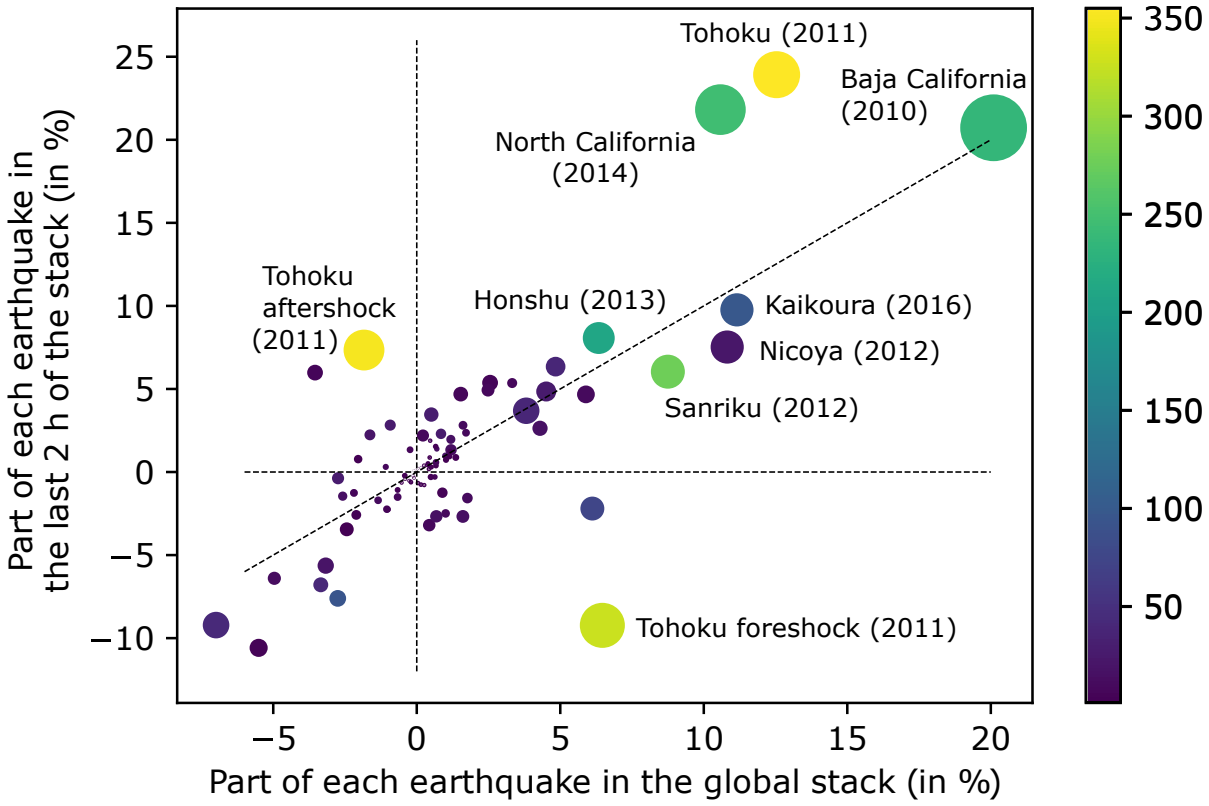

FIGURE S4 – **Earthquakes weights in the stack.** Contribution C_i^{2h} (in %) of each earthquake to the last 2 h of the stack as a function of the contribution C_i^{48h} to the 48 h stack. The dot sizes correspond to the relative values of σ_i for each event. The colors represent the number of stations available for each earthquake. The dashed line shows the axis where $C_i^{2h} = C_i^{48h}$. Event names are given for earthquakes with $\sigma_i > 4\%$.

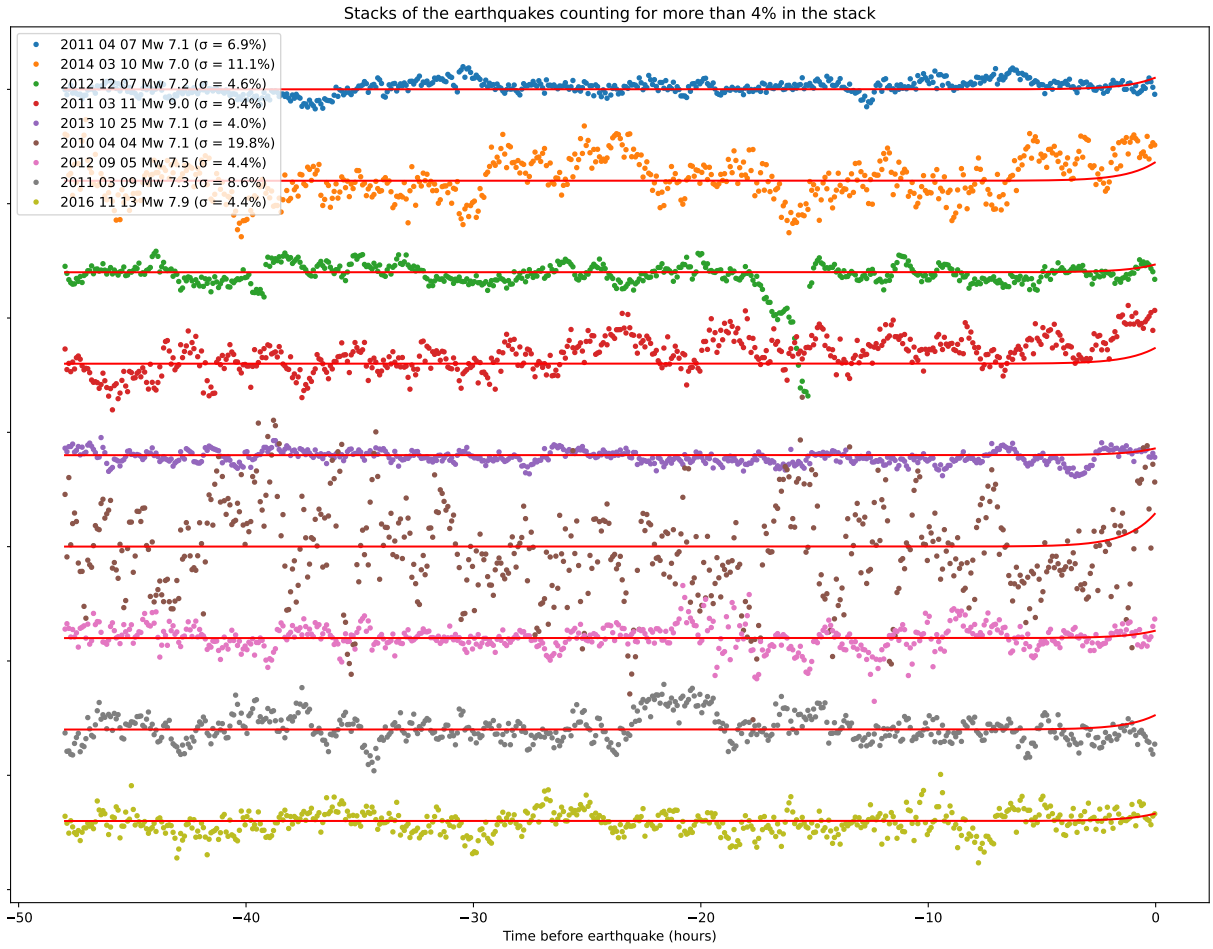

FIGURE S5 – **Stack by earthquake.** Individual stacks for earthquakes with $\sigma_i > 4\%$, i.e. earthquakes counting for more than 4% in the global stack (events highlighted in Fig. S4). Red curves show the exponential fit weighted by σ_i. See the GitHub repository (eq_stack_figures folder) for the plots of the complete list of earthquakes.

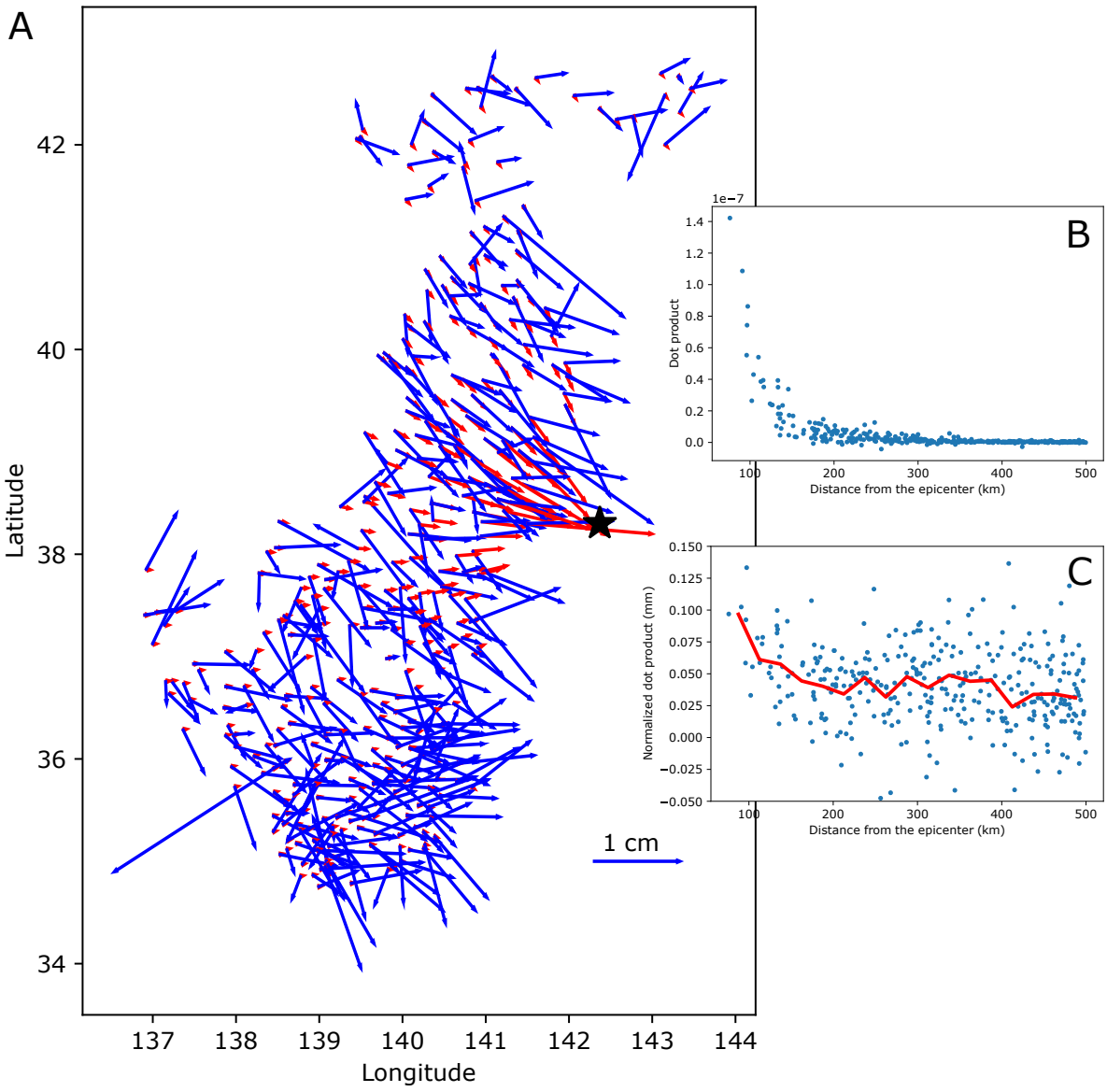

FIGURE S6 – **Map view of the observed and expected displacements for Tohoku.** (A) Observed median displacements (blue arrows) in the 2 hours preceding the Tohoku earthquake with respect to the median position on the previous day and synthetic displacements (red arrows) expected from hypothetical pre-slip at the epicenter of the upcoming Tohoku earthquake (black star). (B) Dot products of the blue and red arrows as a function of distance from the epicenter. (C) Same as (B) normalized by the the norm of the expected displacements, with a 25 km moving averaged superimposed (red curve).

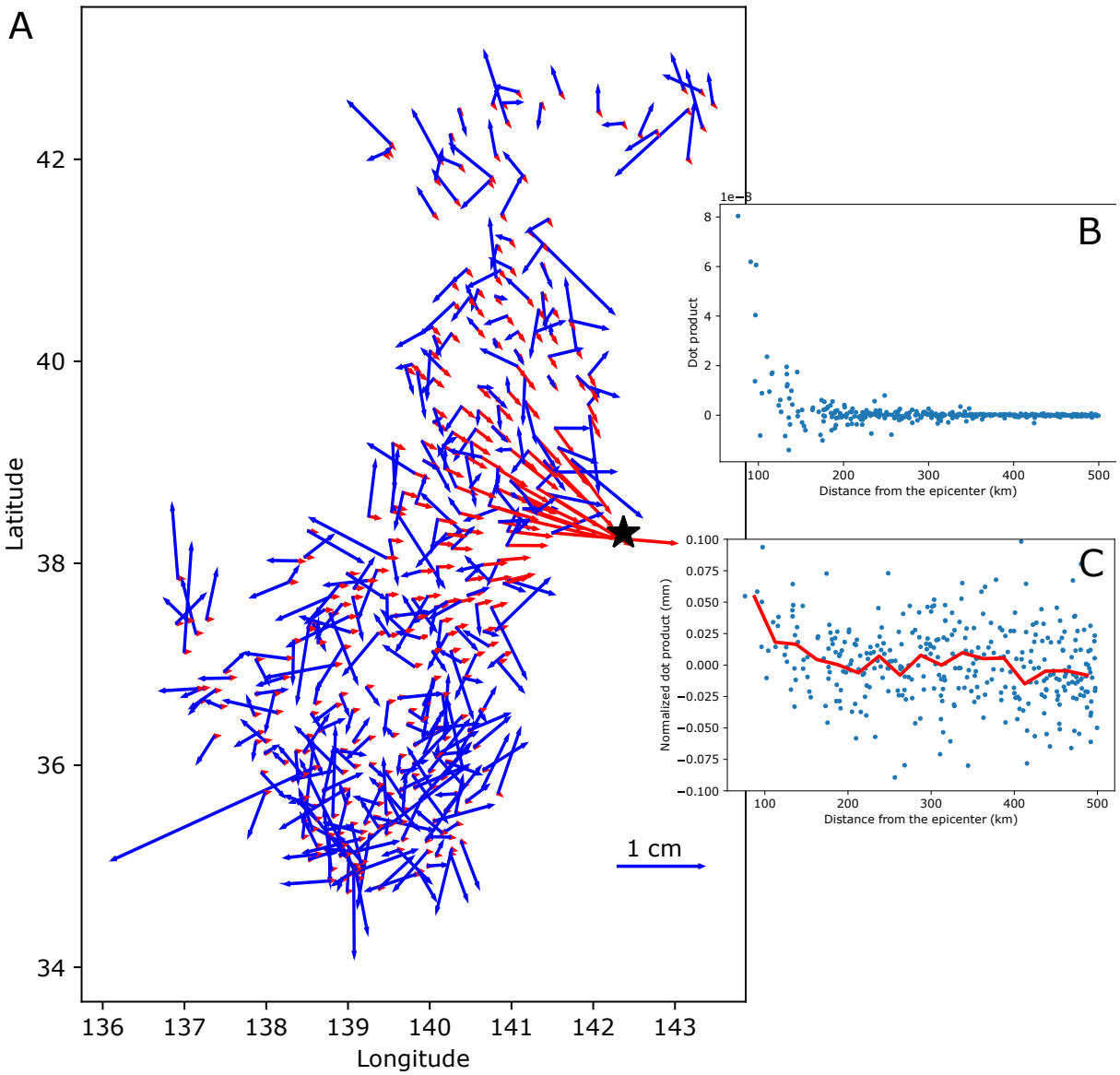

FIGURE S7 – **Same as Fig. S6 after removing the common mode.**

FIGURE S8 – **Global stack as a function of distance.** Global stack calculated using only stations within 100 km (A), 200 km (B), 300 km (C), 400 km (D) and 500 km (E) from the epicenter. Differences are marginal because the amplitude of the Green's functions naturally damps the weight of distant stations.

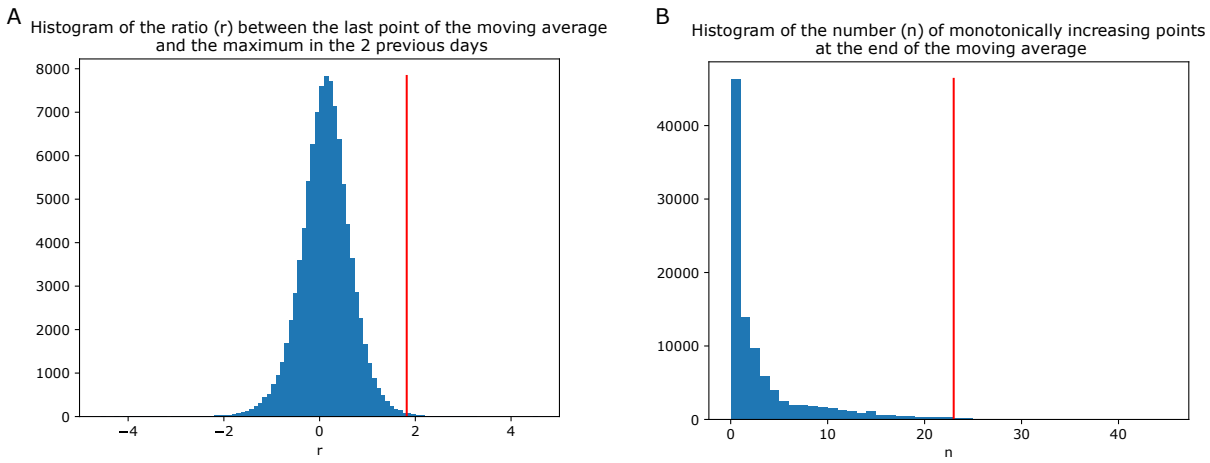

FIGURE S9 – **Uniqueness of the exponential signal in the global stack.** (A) Histogram of the ratio r between the last point of the moving average and its maximum in the preceding 48 hours for 100,000 random combinations of dot product stacks drawn at random times. (B) Histogram of the number n of monotonically increasing points at the end of the moving average for the same 100,000 random combinations of dot product stacks drawn at random times. The vertical red lines show the values observed in the moving average preceding large earthquakes.

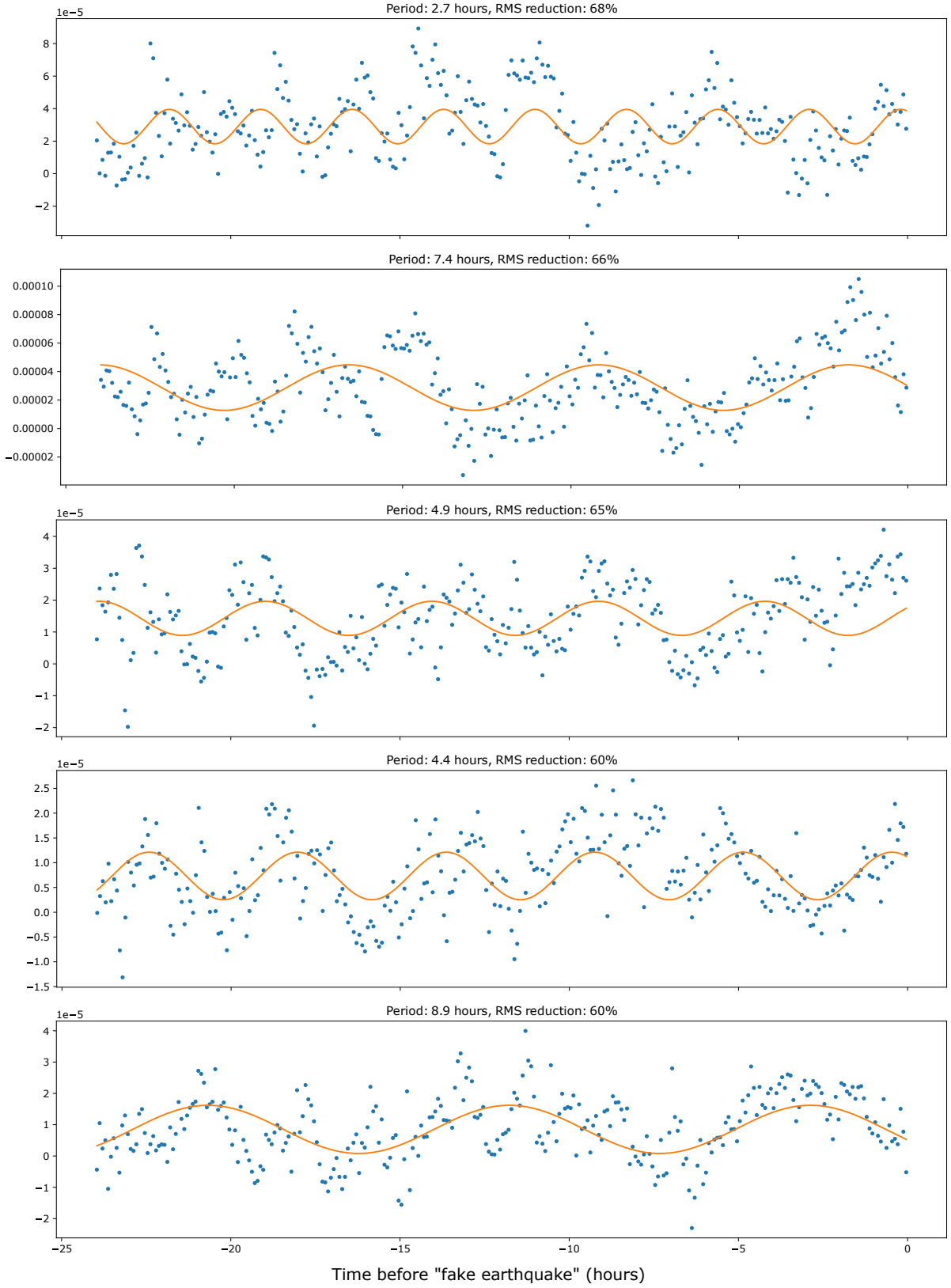

FIGURE S10 – **Uniqueness of the sinusoidal signal preceding Tohoku.** Sinusoidal fits with misfit reduction above 60% and period below 10 hours obtained over 833 stacks made at random times. None exceeds the 72% of misfit reduction found before the Tohoku earthquake.

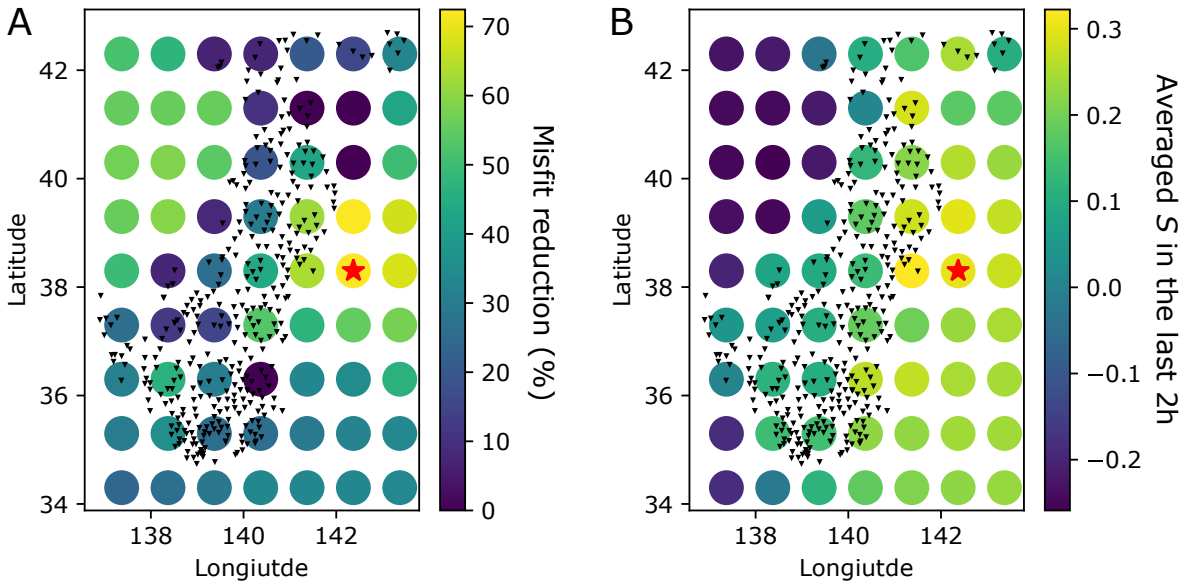

FIGURE S11 – **Location of the source of the periodic and exponential signals before Tohoku.** (A) Misfit reduction of the sinusoidal function (of any period) best fitting the stacks computed moving the source location. The red star shows the location of the Tohoku-Oki earthquake. The inverted black triangles show the location of the GPS stations. (B) Same as (A) for the averaged value in the last 2 h of the stacks computed considering different synthetic source location.